

Infrared Spectroscopic Characterization of Lipid–Alkylsiloxane Hybrid Bilayer Membranes at Oxide Substrates

Atul N. Parikh,^{*,†} Jaime D. Beers,^{†,‡} Andrew P. Shreve,[§] and Basil I. Swanson^{*,†}

Chemical Science & Technology Division, Los Alamos National Laboratory,
Los Alamos, New Mexico 87545

Received October 1, 1998. In Final Form: February 11, 1999

Successive depositions of precompressed Langmuir monolayers have been shown to allow reproducible formation of air-stable, lipid–alkylsiloxane hybrid bimolecular architectures at oxidic supports. Specifically, prepolymerized Langmuir–Blodgett films of *n*-octadecylsiloxane (OTS) monolayers on oxidized silicon substrates were used as the hydrophobic templates, upon which compressed monolayers of dipalmitoyl-*sn*-1-glycerophosphatidylcholine (DPPC) and monosialogangliosides (Gm1) were deposited from a low-temperature air–water interface by the horizontal deposition method. Structural features of each leaflet of the resultant bimolecular architectures, namely DPPC/OTS/SiO₂/Si and Gm1/OTS/SiO₂/Si, were characterized using a combined application of infrared spectroscopy, null-ellipsometry, and surface wetting measurements. In both cases, the outer lipid leaflet (DPPC or Gm1) was found to be structurally decoupled with respect to the inner OTS layer. The inner silane layer was composed of essentially untilted (cant angle, $\theta = 0\text{--}10^\circ$), all-trans chains at the dense packing of $\sim 19 \text{ \AA}^2/\text{molecule}$, consistent with the previously reported structure in solution-phase assembled OTS monolayers. The outer DPPC leaflet, however, was found to be composed of collectively tilted ($\theta = 36^\circ$), all-trans acyl chains at the lower chain-packing density ($\sim 26\text{--}28 \text{ \AA}^2/\text{chain}$) whereas the outer Gm1 leaflet was concluded to have essentially untilted chains at similarly lower chain-packing densities ($\sim 23\text{--}26 \text{ \AA}^2/\text{chain}$) but with the carbohydrate head-groups disposed in a topologically staggered conformation. The structural independence of the two leaflets in the two classes of bilayered architectures examined here confirms the possibility of independently manipulating the molecular structure in each leaflet of supported hybrid bilayers.

1. Introduction

Stable membrane-mimetic architectures (MMAs) on solid-supporting substrates are becoming increasingly important for applications that include biosensor devices,¹ preparation of biocompatible surfaces,² and fundamental biophysical studies of membranes.³ For these applications, MMAs must meet a set of stringent requirements. In the most desirable case, supported membranes would have a high degree of stability, in either aqueous or dry environments, but would maintain the two-dimensional fluidity appropriate for biological membranes.⁴ Also, in many cases (e.g., biosensors), the MMA must be multicomponent, for example, containing both phospholipids and receptor molecules. General preparation strategies that allow for the fabrication of molecularly multicomponent MMAs that satisfy the stability and fluidity requirements are just

emerging,^{5–8} and there remains a need for exploration of preparation strategies and substrate materials, along with use of a full array of characterization techniques.

A number of useful approaches for the preparation of MMAs have been developed over the last several years. These include vesicle spreading onto substrate surfaces,⁵ Langmuir–Blodgett depositions (horizontal and vertical transfers),^{6–7} and molecular self-assembly from dilute organic solutions.⁸ The supported MMAs obtained thus far can be divided into three categories: (1) single, supported lipid bilayer membranes (s-BLMs), prepared by vesicle spreading or LB deposition at hydrophilic

* Corresponding authors. E-mail addresses: basil@lanl.gov, parikh@lanl.gov.

[†] Advanced Instrumentation & Diagnostics Group, CST-1.

[‡] Participant, Underrepresented & Minority Student Program, Los Alamos National Laboratory.

[§] Bioscience & Biotechnology Group, CST-4.

(1) (a) Special Issue on Artificial Biosensing and Interfaces: Surface Modification and Characterization. *Biosens. Bioelectron.* **1995**, *10* (9–10). (b) Tien, H. T. *Adv. Mater.* **1990**, *2*, 316–318. (c) Tien, H. T. *Prog. Surf. Sci.* **1985**, *19*, 169–274.

(2) (a) Radler, J.; Sackmann, E. *Curr. Opin. Solid State Mater. Sci.* **1997**, *2*, 330–336. (b) Tien, H. T.; Salamon, Z.; Ottova, A. *Crit. Rev. Biomed. Eng.* **1991**, *18*, 323–340. (c) Chaikof, E. L. *Chemtech* **1996**, *26*, 17–22.

(3) (a) Spinke, J.; Liley, M.; Guder, H. J.; Angermaier, L.; Knoll, W. *Langmuir* **1993**, *9*, 1821–1825. (b) Liley, M.; Bouvier, J.; Vogel, H. J. *Colloid Interface Sci.* **1997**, *194*, 53–58. (c) Salafsky, J.; Groves, J. T.; Boxer, S. G. *Biochemistry* **1996**, *35*, 14773–14781.

(4) (a) Puu, G.; Gustafson, I. *Biochim. Biophys. Acta–Biomembr.* **1997**, *1327*, 149–161. (b) Boggs, J. M. *Biochim. Biophys. Acta* **1987**, *906*, 353–404 and selected references therein.

(5) (a) Bayerl, Th. M.; Bloom, M. *Biophys. J.* **1990**, *58*, 357–368. (b) Kalb, E.; Frey, S.; Tamm, L. K. *Biochim. Biophys. Acta* **1992**, *1103*, 307–316.

(6) (a) Tamm, L. K.; McConnell, H. M. *Biophys. J.* **1985**, *47*, 105–113. (b) Merkel, R.; Sackmann, E.; Evans, E. J. *J. Phys. (Paris)* **1989**, *50*, 1535–1555.

(7) (a) Plant, A. L. *Langmuir* **1993**, *9*, 2764–2767. (b) Miller, C.; Cuendet, P.; Gratzel, M. J. *Electroanal. Chem.* **1990**, *278*, 175–192. (c) Florin, E.-L.; Gaub, H. E. *Biophys. J.* **1993**, *64*, 375–383. (d) Pierrat, O.; Lechat, N.; Bourdillon, C.; Laval, J. M. *Langmuir* **1997**, *13*, 4112–4118. (e) Ding, L.; Li, J. H.; Dong, S. J.; Wang, E. K. *J. Electroanal. Chem.* **1996**, *416*, 105–112. (f) Williams, L. M.; Evans, S. D.; Flynn, T. M.; Marsh, A.; Knowles, P. F.; Bushby, R. J.; Boden, N. *Supramol. Sci.* **1997**, *4*, 513–517. (g) Lingler, S.; Rubinstein, I.; Knoll, W.; Offenhäusser, A. *Langmuir* **1997**, *13*, 751–757. (h) Lingler, S.; Rubinstein, I.; Knoll, W.; Offenhäusser, A. *Langmuir* **1997**, *13*, 7085–7091. (i) Cheng, Y. L.; Boden, N.; Bushby, R. J.; Clarkson, S.; Evans, S. D.; Knowles, P. F.; Marsh, A.; Miles, R. E. *Langmuir* **1998**, *14*, 839–844.

(8) (a) Lang, H.; Duschl, C.; Vogel, H. *Langmuir* **1994**, *10*, 197–210. (b) Cornell, B. A.; Braasch-Makszytytis, V. L. B.; King, L. G.; Osman, P. D. J.; Raguse, B.; Wiczorek, L.; Pace, R. J. *Nature* **1997**, *387*, 580–583. (c) Raguse, B.; Braasch-Makszytytis, V. L. B.; Cornell, B. A.; King, L. G.; Osman, P. D. J.; Pace, R. J.; Wiczorek, L. *Langmuir* **1998**, *14*, 648–659. (d) Duschl, C.; Sevinlandais, A. F.; Vogel, H. *Biophys. J.* **1996**, *70*, 1985–1995. (e) Duschl, C.; Liley, M.; Lang, H.; Ghandi, A.; Zakeeruddin, S. M.; Stahlberg, H.; Nemetz, A.; Knoll, W.; Vogel, H. *Mater. Sci. Eng., C* **1996**, *4*, 7–18.

surfaces; (2) single, covalently tethered, self-assembled monolayers (t-SAMs) of functionalized lipid derivatives, prepared by solution-phase coadsorption of membrane-forming components; and (3) asymmetric or hybrid bilayer membranes (HBMs), composed of an outer lipid layer and an inner, substrate-bound, self-assembled monolayer, prepared by an initial application of molecular self-assembly followed by either vesicle spreading or a Langmuir–Schaeffer deposition of lipids. The most natural membrane bilayer environment is probably represented by s-BLMs, for, in this case, a hydration layer (or comparable hydrophilic cushion) separates the bilayer from the substrate. This leads to a fully bilaterally hydrated architecture which also retains the two-dimensional fluidity typical of biological membranes. However, the structural integrity of s-BLMs is strongly dependent on the presence of the ambient medium (i.e., an aqueous environment is required for good stability), which can limit their practicality in some applications. In addition, since many applications do not require a bilaterally hydrated membrane assembly, one may consider increasing membrane stability by incorporating direct coupling of the MMA to the substrate. The extreme case of this approach is a t-SAM, in which a monolayer is attached to a solid substrate via epitaxial coordination or covalent bonding. These monolayers are structurally robust, maintaining their integrity in a wide range of aqueous and nonaqueous liquid environments and also after being dried. This stability, however, is obtained by sacrificing fluidity, and t-SAMs have a biologically unrealistic structural rigidity that can be limiting in many applications. Thus, an attractive alternative is HBMs. Here, stability is derived both by surface attachment as in t-SAMs and by van der Waals interactions between the lipid tails and interactions between the lattices of CH₃ end groups of the two layers as in s-BLMs. In principle, this balance of properties leads to an increase in stability compared to that of s-BLMs but with a possibility of retention of fluidity within the outer leaf. In addition, the outer and inner leaves of the bilayer architecture can be independently manipulated.

The structural possibilities and potential applications offered by HBMs have yet to be fully explored. While HBMs on various oxide surfaces have been used in various applications (e.g., FTIR studies),^{9,10} previous studies of the structure and organization in HBMs have primarily focused on HBMs composed of phospholipid–alkanethiol assemblies on a polycrystalline gold surface. Plant and co-workers used surface plasmon resonance¹¹ and AC impedance spectroscopy¹² to establish such HBMs as an appropriate model membrane matrix for probing ligand–receptor interactions and to demonstrate that their electrical characteristics were consistent with biological membranes. Recently, the same group has provided a molecular level description of structure in these phospholipid–alkanethiol HBMs using a combined application of reflection–absorption infrared spectroscopy (RAIRS), surface-enhanced Raman spectroscopy (SERS), atomic force microscopy (AFM), and neutron reflectivity (NR) measurements.¹³ The phospholipid leaflet was found to be a macroscopically homogeneous monolayer with mo-

lecular order commensurate with that observed in s-BLMs, and further, the lipid layer was determined to be highly oriented with its phosphocholine (PC) group lying at the ambient interface. Construction of the HBM resulted in only a minor restructuring of the initial thiol layer, and in the outer phospholipid layer the average acyl chain was canted at $\sim 34^\circ$ from the surface normal, in close parallel to the average cant angles of $28\text{--}34^\circ$ of the alkanethiol inner leaf.¹⁴ A related preparation demonstrated by Cornell et al.^{8b,8c} is to use selective thiol linkages to tether a true phospholipid bilayer to a gold substrate but with an intervening aqueous cushion. This approach could potentially combine all of the advantages of s-BLMs, including the possibility of studying membrane-transport phenomena, with the stability of HBMs, and indeed, Cornell and co-workers report a high degree of stability for the MMA that they have developed, and demonstrate its use as a sensor platform with transduction based on transmembrane ionic conduction.^{8b,c}

While this previous work illustrates the development and characterization of HBMs on gold surfaces, there are many reasons for developing general and well-characterized approaches to make HBMs on oxide substrates. For example, such HBMs would be important in biosensor applications in which optical transduction is done using waveguiding methods.^{15,16} In addition, oxide surfaces in many different morphologies are easily obtained. Thus, for example, flow cytometry studies could use HBMs developed on glass microspheres,¹⁷ but corresponding experiments using metal beads would be difficult. Another motivation is provided by the potential for increased control of the structure of HBMs, especially multicomponent HBMs, on oxide surfaces. The inner, self-assembled, leaflet on oxide surfaces typically consists of a monolayer of long-chain trifunctional silanes. Recent efforts^{18,19} have demonstrated the possibility of structural control in such monolayers by transferring prepolymerized precursors²⁰ from an air–water interface. These studies have indicated that silane monolayers transferred from their Langmuir phase precursors can be manipulated to form a number of structurally different morphologies including islanded films, porous films, and homogeneous liquid-like films simply by altering the sub-phase pH and temperature. Such varied monolayer architectures are difficult to obtain in a controlled manner using classical, solution-phase, self-assembly techniques for alkanethiols. Further, the horizontal deposition technique for the transfer of lipid overlayers is also suited to preparing

(9) Linseisen, F. M.; Hetzer, M.; Brumm, T.; Bayerl, T. M. *Biophys. J.* **1997**, *72*, 1659–1667.

(10) (a) Axelsen, P. H.; Citra, M. J. *Prog. Biophys. Mol. Biol.* **1997**, *66*, 227–253 and selected references therein. (b) Tamm, L. K.; Tatulian, S. A. *Q. Rev. Biophys.* **1997**, *30*, 365–429.

(11) Plant, A. L.; Brigham-Burke, M.; O'Shannessy, D. *Anal. Biochem.* **1995**, *226*, 342–348.

(12) Plant, A. L.; Guegutchkeri, M.; Yap, W. *Biophys. J.* **1994**, *67*, 1126–1133.

(13) (a) Meuse, C.; Krueger, S.; Majkrzak, C. F.; Dura, J. A.; Fu, J.; Connor, J. T.; Plant, A. L. *Langmuir* **1998**, *74*, 1388–1398. (b) Meuse, C. W.; Niaura, G.; Lewis, M. L.; Plant, A. L. *Langmuir* **1998**, *14*, 1604–1611.

(14) (a) Laibinis, P. E.; Whitesides, G. M.; Allara, D. L.; Tao, Y.-T.; Parikh, A. N.; Nuzzo, R. G. *J. Am. Chem. Soc.* **1991**, *113*, 7152–7167. (b) Fenter, P.; Eisenberger, P.; Liang, K. S. *Phys. Rev. Lett.* **1993**, *70*, 2447–2451.

(15) (a) Beswick, R. B.; Pitt, C. W. *J. Colloid Interface Sci.* **1988**, *124*, 146. (b) Zhao, S.; Reichert, W. M. *Langmuir* **1992**, *8*, 2785.

(16) (a) Heidemann, R. G.; Kooyman, R. P. H.; Greve, J. *Sens. Actuators* **1991**, *B4*, 297–299. (b) Lukosz, W.; Stamm, C. H. *Sens. Actuators* **1991**, *A25–27*, 185–188.

(17) See, for example: (a) Obringer, A. R.; Rotes, N. S.; Walter, A. *J. Immunol. Methods* **1995**, *185*, 81–93. (b) Eschwege, V.; Laude, I.; Toti, F.; Pasquali, J. L.; Freyssinet, J. M. *Clin. Exp. Immunol.* **1996**, *103*, 171–175.

(18) Wang, R.; Parikh, A. N.; Beers, J. D.; Shreve, A. P.; Swanson, B. I. Submitted for publication.

(19) (a) Parikh, A. N.; Wood, J.; Sharma, R.; Allara, D. L. *ACS Symp. Ser.* **1995**, *615*, 355–363. (b) Kojio, K.; Ge, S. R.; Takahara, A.; Kajiyama, T. *Langmuir* **1998**, *14*, 971–974. (c) Ge, S. R.; Takahara, A.; Kajiyama, T. *Langmuir* **1995**, *11*, 13411–1346.

(20) (a) Ariga, K.; Okahata, Y. *J. Am. Chem. Soc.* **1989**, *111*, 1148. (b) Barton, S. W.; Goudot, A.; Rondelez, F. *Langmuir* **1991**, *7*, 1029–1031.

structured outer leaflets for the HBMs (although this advantage could also be exploited for HBMs on metal substrates). Taken together, the two Langmuir-phase assisted assembly techniques should allow, on oxide substrates, the formation of variously structured, multi-component, and structurally independent outer and inner leaves in an HBM architecture.

With this motivation, we have initiated studies to fabricate and characterize HBMs at oxide surfaces. We report a preparation procedure that uses a precursor Langmuir phase for the formation of an octadecylsiloxane-anchored inner leaf on a silicon substrate (with a native oxide overlayer), followed by a horizontal (Langmuir-Schaeffer) transfer of a long-chain phospholipid (DPPC) or glycolipid (Gm1) as an outer leaflet. In this study, an LB method is used for silanization of a silicon substrate to obtain a highly homogeneous silane inner leaf, while the horizontal transfer of surface-condensed phases leads to preparation of HBMs in a nominally dry state. The choice of DPPC and Gm1 for the outer leaf was motivated both by their presence in cell membranes and by the availability of comprehensive literature detailing their phase behavior at the air-water interface.²¹ The structure and properties of the HBMs Gm1/OTS/SiO₂/Si and DPPC/OTS/SiO₂/Si (OTS = octadecyltrichlorosilane) were then determined using transmission infrared spectroscopy with quantitative analysis, single-wavelength null-ellipsometry, and wetting measurements, while the surface pressure dependent properties of the precursor Langmuir phases (prior to their transfer onto the solid supports) were assessed using surface pressure-area phase diagrams. These studies provide insight on the importance of head-group and chain-chain interactions in determining the molecular structure of the films and demonstrate that the inner and outer leaflets in these HBM assemblies are discommensurate and can therefore be independently manipulated.

2. Experimental Section

2.1. Materials. Dipalmitoyl-*sn*-glycero-3-phosphocholine (DPPC; Avanti Polar-Lipids, Alabaster, AL) and high-purity monosialoganglioside (Gm1; Matreya, Inc., Pleasant Gap, PA) were obtained from commercial sources and used without further purification. Octadecyltrichlorosilane (OTS) of >95% purity was obtained from Aldrich (St. Paul, MN), and the solvents chloroform and methanol were HPLC grade with the manufacturer's (Fisher Scientific) listed purity of at least 99%. Organic-free deionized water of high resistivity (>16.0 m Ω ·cm) was obtained by processing water through a Millipore purification system (Bedford, MA) consisting of a reverse-osmosis deionization cartridge and an ion-exchange/carbon purification system. All glassware used was thoroughly pre-cleaned using chromic/sulfuric acid or base-bath solutions followed by extensive washing with deionized, low-organic-content water and finally air-drying in a glassware oven maintained at 160 °C. The silicon substrates with a native oxide overlayer (SiO₂/Si) were obtained from Harrick Scientific (Ossining, NY) as 1 in. thick square plates. Both sides were finished to a high polish, and one side was wedged slightly off-parallel from the other by 0.25° in order to minimize the interference fringes in the transmission infrared spectroscopy measurements.

2.2. Sample Preparation. Substrate Pretreatments. All new silicon substrates were thoroughly degreased by ultrasonication in CHCl₃ for ~5 min. The samples were then oxidized²² using a combination of chemical (*piranha-etch* treatment) and photochemical (UV/ozone oxidation) treatments such that the final

step was always photochemical. The *piranha-etch* treatment involved immersing the samples for a period of 5–10 min in a freshly prepared 4:1 v/v mixture of sulfuric acid (A300-500, Fisher Certified ACS+, Fairlawn, NJ) and hydrogen peroxide (30% Baker Analyzed solution, J. T. Baker, Phillipsburg, NJ) maintained at ~100–110 °C. (*Caution: this mixture reacts violently with organic materials and must be handled with extreme care.*) The samples were then withdrawn using Teflon tweezers, rinsed immediately with copious amounts of organic-free, deionized water, and finally dried under a stream of nitrogen. The UV/ozone treatment²³ was carried out using a commercial UV/ozone reactor (Model UV CLEAN 135500, Boekel Scientific, Feasterville, PA). The samples were exposed to the ozone-generating (187–254 nm) lamp-grid for ~10–15 min. Previously used silicon samples were occasionally recycled by first stripping the oxide layer by exposing it to a buffered ammonium hydrogen fluoride solution (Improved Buffer HF system, Transene Co., Rowley, MA) for ~45–60 s, followed by forming a pristin oxide layer using the combination of chemical and photochemical processes detailed above. Freshly oxidized samples were then utilized for film transfers within 5–10 min of the above pretreatment process.

Vertical LB Deposition of OTS Monolayers. A modification of a previously published procedure for the transfer of prepolymerized monolayers from OTS molecules spread at the air-water interface of a constant-perimeter trough was used.¹⁹ Briefly, over a freshly aspirated and slightly acidic subphase (pH = 5.8) prepared using deionized water, a 25–50 μ L aliquot of 1 mg/mL octadecyltrichlorosilane (OTS) in chloroform was spread dropwise. The solution was allowed to stand for ~40 min in order to allow complete evaporation of the solvent and for equilibrium hydrolysis and polymerization of the trichlorosilyl head-group to occur. The subphase temperature during the isotherm run was held constant at 15 or 25 °C to an accuracy of ± 0.3 °C. OTS monolayers were transferred at a surface pressure of 35 mN/m and a vertical pulling rate of 10 mm/min. The Teflon trough used was a computer controlled, 600 cm² Langmuir-Blodgett system (Model 611D2, NIMA Technologies, Coventry, England) with Teflon-coated moving barriers. The pressure measurements were by the Wilhelmy plate method. The subphase pH was monitored using a pH sensor (EDT Instruments, model GP353, Kent, England), and the temperature of the subphase medium was controlled to within ± 0.5 °C using a circulating water bath (VWR Scientific, model 1157, Niles, IL). The temperature of the ambient medium (air) was not controlled but was monitored to be 20.4 \pm 0.4 °C for all measurements reported here.

Horizontal Deposition of Lipid Overlayers. Solutions of DPPC and Gm1 were spread drop-by-drop from a chloroform-cleaned, glass microsyringe (Hamilton) onto the near-neutral subphase surface of pure, deionized water. The lipid solutions were nominally 1 mg/mL, and 25–100 μ L solution was applied to the subphase surface. The subphase surfaces were then left unattended or stirred using magnetic stirrers for ~20–30 min to ensure complete evaporation of the solvent phase. Compression (as well as expansion) isotherms were subsequently collected in a quasi-static mode by moving the surface barriers at velocities of 10–25 cm²/min. Single DPPC and Gm1 monolayer transfers to the solid substrate were carried out at the surface pressure 25 mN/m by the Langmuir-Schaeffer or horizontal touch method.²⁴ Horizontally aligned OTS-coated substrates were lowered until a visible meniscus was observed to form a continuous contact across the substrate surface. After a contact time of ~5 min, the substrates were slowly raised (2–3 mm/min) till the contact with the air-water interface was observed to break. The transfer ratios, which were always found to be in a close vicinity of 100%, appear to indicate the transfer of a single monolayer under the conditions employed.²⁵ The samples were then placed in polypropylene (Fluoroware) containers stored in a laboratory desiccator before final characterization.

(23) Vig, J. R. *J. Vac. Sci. Technol. A* **1985**, *3*, 1027–1033.

(24) Lee, S.; Virtanen, J. A.; Virtanen, S. A.; Penner, R. M. *Langmuir* **1992**, *8*, 1243–1246.

(25) It is interesting to note that all OTS, Gm1, and DPPC layers were transferred onto the hydrophobic OTS-coated silicon substrates as single layers alone. A previous study by Lee and co-workers²⁴ has shown that typical fatty acids, in contrast, transfer onto the hydrophobic solids as integral multiples of bilayers.

(21) See, for example: (a) Marsh, D. *Chem. Phys. Lipids* **1991**, *57*, 109–120 and references therein. (b) Boretta, M.; Cantu, L.; Corti, M.; del Favero, E. *Physica A* **1997**, *236*, 162–176 and selected references therein. (c) Boullanger, P. *Top. Curr. Chem.* **1997**, *187*, 275–312.

(22) Frantz, P.; Granick, S. *Langmuir* **1992**, *8*, 1176–1182.

2.3. Characterization. Contact Angle Measurements. Wetting measurements were carried out to determine the surface free energy of the silane-coated substrates. Water and a set of *n*-alkanes were used as probe liquids using a standard goniometric apparatus (Ramé-Hart Model 100, Mountain Lakes, NJ). Static drops (10–30 μ l) were delivered from a flat-tipped micropipet, and the measurements were performed under a saturated vapor of the probe liquid in a controlled atmosphere chamber. The reported values are averages of those for three different drops on each sample surface. Spot-to-spot variation on a given sample was less than $\pm 2^\circ$, and the overall accuracy in the measurements was less than $\pm 3^\circ$. To determine advancing and receding contact angles simultaneously, the substrate stage was slowly tilted until the drop began to move by gravity. The forward and trailing edges of the drop just before it begins to translate at the sample surface provide simultaneous measures of the advancing and receding angles. The errors in these measurements were typically $\pm 4^\circ$. The advancing contact angles then were used to derive the critical surface tension (γ_c) values of the monolayers using the well-known Zisman method.²⁶

Single-Wavelength Ellipsometry. A null-ellipsometer (model AutoEl III, Rudolph Research, Fairfield, NJ) operating at 632.8 nm and at a 70° angle of incidence was used with a beam spot of ~ 2 mm to estimate the film thickness²⁷ for all OTS, DPPC, and Gm1 layers. Measurements were made at three different spots on each sample. The ellipsometric parameters, namely phase shift (Δ) and amplitude ratio (Ψ), respectively, were recorded. The instrumental precision of the ellipsometric angles was 0.04° , and the overall, sample-to-sample errors in terms of final calculated film thicknesses, as detailed below, are within ± 2 Å.

Film thicknesses were determined from the ellipsometric parameters using standard electromagnetic treatment for a parallel-layer model consisting of an air/aliphatic chain/head-group/substrate structure. The film thickness was determined using independently assigned values of the substrate and film optical functions (or dielectric constants). The substrate phase (hence designated as SiO₂/Si), composed of amorphous oxide and crystalline silicon phases, any adsorbed water phase are treated as optically isotropic and thus assigned scalar optical (or dielectric) functions. The pseudodielectric constant for the above SiO₂/Si layer was derived conveniently by analyzing the experimental measurement of the ellipsometric angles for the freshly cleaned, hydrated, oxidized SiO₂/Si sample using a two-phase model.²⁷ In contrast, since the organic films are expected to consist (see results) of oriented aliphatic chains, these were considered as optically anisotropic phases. Further, since the OTS, DPPC, or Gm1 films exhibit no optical absorption at 632.8 nm, the optical function is a real quantity, and since at the length scale of the measurements (2 mm spot size) the densely packed LB layers are structurally hexatic or optically uniaxial,²⁸ the film optical tensor is described adequately by two independent real constants, namely ordinary (n_o) and extraordinary (n_e) refractive indices. The actual calculations followed a rigorous algorithm based on matrix formulations of the associated electromagnetic equations, and details can be found elsewhere.²⁹

For the OTS film layer, the isotropic calculations³⁰ were performed by assuming the refractive index was the isotropic average value $n_i = \frac{1}{3}(2n_o + n_e)$ for the entire length of the molecule l , estimated from the previously reported values of $n_o = 1.474$ and $n_e = 1.554$. For more rigorous anisotropic calculations, the OTS film layer was modeled to consist of two separate slabs, head-group h and aliphatic tail l , such that $l = l + h$. For the aliphatic tail slab, the separate values of ordinary and extraor-

dinary refractive indices, namely $n_o = 1.484 + 0i$ and $n_e = 1.559 + 0i$, were used as a first approximation,^{31,32} whereas the value of $1.50 + 0i$ was retained for the siloxane head-group. The thickness for the siloxy head-group network was assigned using molecular models to be ~ 3 – 4 Å. For the DPPC and Gm1 film layers, the isotropic calculations were performed using the refractive indexes $1.44 + 0i$ and $1.402 + 0i$, respectively, for the entire layer. These values were obtained from the results of surface force measurements by Luckham et al.³³ Optical constants for the head-group slabs, composed of the PC and the pentasaccharide (PS) head-groups for the DPPC and the Gm1 films, respectively, were approximated by the isotropic optical constants of bulk water, since these head-groups retain a significant amount of water in their matrix³¹ ($n = 1.3313 + 0i$). Strictly speaking, this assumption is not entirely correct, especially since no special care was taken to deliberately keep our samples hydrated, but provides a reasonable approximation. Optical functions for the tail slabs of Gm1 and DPPC monolayers were approximated by the values $n_o = 1.516 + 0i$ and $n_e = 1.570 + 0i$ for the condensed phases of DPPC monolayers at the air–water interface.^{32b}

Infrared Spectroscopy Measurements. Transmission infrared spectra were obtained using a Fourier transform spectrometer (Bruker Optics, Equinox IFS 55, Tubingen, Germany) operating at 4 cm⁻¹ resolution with an unpolarized, convergent beam transmitting through the sample surface at a nominally normal incidence angle. The beam diameter at the focus was controlled at 5 mm by an aperture. The resulting interferograms from multiple, co-added, scans were Fourier transformed with the Blackman–Harris three-term apodization technique and zero-filled to increase the point density by a factor of 4, which yields an effective resolution of ~ 0.5 cm⁻¹ for an accurate determination of the peak positions. The spectra of the OTS samples were referenced against the spectra obtained for the same clean, bare substrate wafers just prior to film deposition, and the difference spectra for the lipid–OTS bilayers were referenced against the spectra of the OTS films.

To deduce molecular orientations from the spectral intensities (and their relative distribution), quantitative comparison of the observed spectra was made with a model spectrum. The model spectrum is obtained by constructing a physical model for the interaction of light with the sample for the experimental geometry using classical electromagnetic theory. The samples are modeled as the nine-layered structure consisting of air/lipid (DPPC or Gm1)/OTS/SiO₂/Si/SiO₂/OTS/lipid (DPPC or Gm1)/air.

The sample attributes required for the calculations include the thicknesses and the dielectric functions of each layer. The average slab thicknesses for the OTS and lipid (DPPC or Gm1) layers are estimated independently using ellipsometric data (see above). The thickness of the SiO₂ layer, also estimated ellipsometrically, was ~ 20 Å, and the silicon wafers had the nominal thickness of ~ 1 mm. The geometrical parameters, normal angle of incidence ($\theta = 0^\circ$) and unpolarized beam, have been chosen to match our experimental procedures (see above). The optical functions of Si and SiO₂ were obtained from the literature³⁴ for the infrared wavelengths whereas the optical constants of the bulk, polycrystalline solids of DPPC, Gm1, and bulk-hydrolyzed OTS molecules were used to represent the isotropic phase of the organic monolayer slabs.³⁵ The isotropic optical functions for the monolayer phases were then transformed into anisotropic optical tensors for an arbitrarily chosen chain orientation as an initial guess. This approach produces explicit simulations of the observed spectra. Any differences between the observed and the calculated spectra were then reconciled by refining the guess for the molecular orientation until the best-fit spectra were obtained. The theoretical basis of these calculations and the justifications

(26) Zisman, W. A. *Adv. Chem. Ser.* **1964**, *43*, 1–51.

(27) (a) Azzam, R. M. A.; Bashara, N. M. *Ellipsometry and Polarized Light*; North-Holland: Amsterdam, The Netherlands, 1977 and selected references therein. (b) Aspnes, D. E. In *Optical Properties of Solids: New Developments*; North-Holland: Amsterdam, The Netherlands, 1976; Chapter 15.

(28) Garoff, S. *Thin Solid Films* **1987**, *49*, 152–168.

(29) Parikh, A. N.; Allara, D. L. In *Spectroscopic Ellipsometry of Heterogeneous Thin Films*; Francombe, M. H., Vossen, J. L., Eds.; Academic Press: New York, 1994; Vol. 19, pp 279–323.

(30) (a) Allara, D. L.; Nuzzo, R. G. *Langmuir* **1985**, *1*, 52–66. (b) McCrackin, F. L.; Passaglia, E.; Stromberg, R. R.; Steinberg, H. L. *J. Res. Natl. Bur. Stand. Sect. A* **1963**, *67*, 363–377.

(31) (a) den Engelsen, D. *Surf. Sci.* **1976**, *56*, 272–280. (b) Ducharme, D.; Max, J.; Saless, C.; Leblanc, R. M. *J. Phys. Chem.* **1990**, *94*, 1990.

(32) (a) Paudler, M.; Ruths, J.; Riegler, H. *Langmuir* **1992**, *8*, 184–189. (b) Thoma, M.; Schwendler, M.; Blates, H.; Helm, C. A.; Pfohl, T.; Riegler, H.; Mohwald, H. *Langmuir* **1996**, *12*, 1722–1728.

(33) Luckham, P.; Wood, J.; Swart, R. *J. Colloid Interface Sci.* **1993**, *156*, 173–183.

(34) *Handbook of Optical Constants of Solids II*; Palik, E. D., Ed.; Academic: Orlando, FL, 1985.

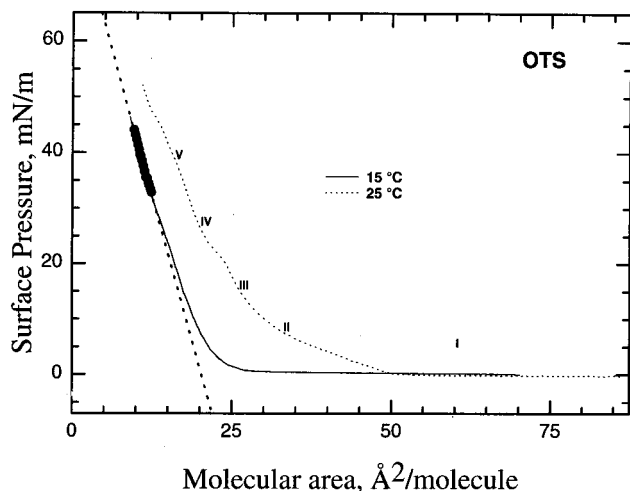


Figure 1. π - A compression isotherm data at 15 and 25 °C for OTS (*n*-octadecyltrichlorosilane) molecules spread at the slightly acidic (pH = 5.8) water subphase.

for the descriptions of the monolayer sample system have been previously described.³⁶

3. Results

3.1. Surface Pressure–Molecular Area Isotherm Measurements. *OTS Monolayers.* The solid trace in Figure 1 shows the typical surface π - A isotherm obtained for monolayers of OTS at the air–water interface at 15 °C and a slightly acidic subphase pH of 5.6. For comparison purposes, the isotherm at the most commonly reported 25 °C is also shown as a dashed curve.^{20,37} The 15 °C isotherm is characterized by two distinct regions including an initial flat portion (I) at ~ 0 mN/m at molecular areas > 25 Å²/molecule (assigned to the G or gas phase) followed by a limb of rapidly rising surface pressures (IV) between the molecular areas ~ 25 and 15 Å²/molecule (assigned to the LC or liquid-condensed phase). Film collapse in companion isotherms occurred (not shown) at ~ 56 mN/m. The 25 °C isotherm, in addition to the general features of the 15 °C isotherm, reveals a weak inflection point (III, assigned to coexisting LE–LC phases) separating the region of gradually rising surface pressures (II) between ~ 50 and ~ 30 Å²/molecule (assigned to the LE or liquid-expanded phase) from the rapidly rising one (IV) between ~ 30 and 25 Å²/molecule (assigned to the LC phase). The assignments above of the I–V general regimes are made in direct analogy with the simplest descriptions of chain amphiphiles at the air–water interface.³⁸ The absence of an LE phase (II and III) in the 15 °C isotherm data for the OTS monolayers indicates that, upon compression, the growth of the OTS film occurs by direct aggregation of LC

(35) Intrinsic isotropic optical functions of the bulk crystallites of solid compounds of hydrolyzed polymers of octadecylsiloxane, DPPC, and Gm1 were determined using independent FT-IR measurements. Here, the samples consisted of pellets prepared by pressing homogenized mixtures of the solid with vacuum-dehydrated pure KBr (spectroscopic Grade, Aldrich) in calculated quantities. The spectra were referenced against the spectra obtained for air or blank KBr pellets under otherwise identical spectrometer conditions and geometry. Optical functions were then determined, as previously described,³⁰ by Beers–Lambert's law in conjunction with a Kramers–Kronig transformation. These values represent an isotropic description of the optical functions of the film layers.

(36) Parikh, A. N.; Allara, D. L. *J. Chem. Phys.* **1992**, *96*, 927–945.

(37) Fang, J. Y.; Knobler, C. M. *J. Phys. Chem.* **1995**, *99*, 10425–10429.

(38) See, for example: (a) Gaines, G. L., Jr. *Insoluble Monolayers at Liquid–Gas Interfaces*; Wiley-Interscience: New York, 1966 and references therein. (b) Knobler, C. M. *Science* **1990**, *249*, 870 and selected references therein.

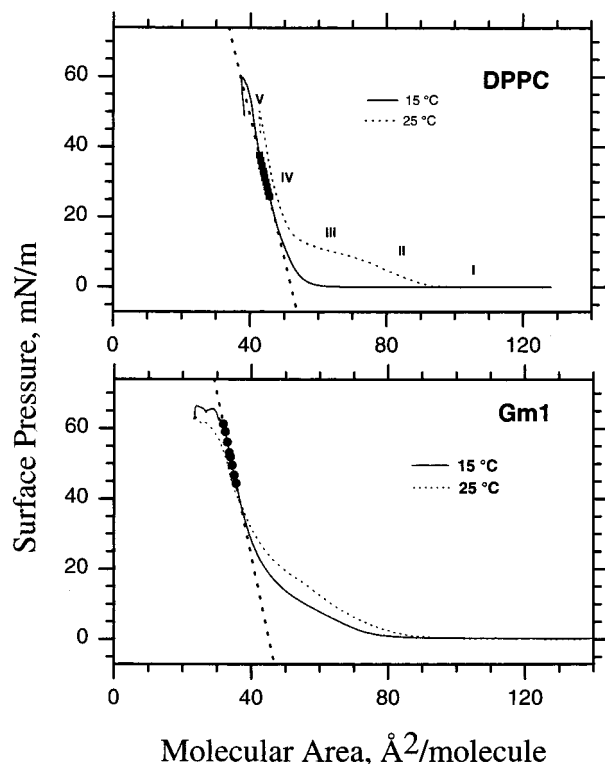


Figure 2. π - A compression isotherms 15 and 25 °C for (a) DPPC and (b) Gm1 molecules spread at the neutral water subphase.

islands via the G–LC transition as opposed to the intermediate conformational ordering that characterizes the LE–LC transition observed in the 25 °C isotherm. The low-temperature film-growth mode is favorable for efficient packing and less defective film structures in the fully compressed films.³⁹ Corroborative evidence in support of this assertion is provided by the significantly lower limiting surface area or A_0 (obtained by extrapolating the LC limb region to 0 mN/m surface pressure) obtained for the 15 °C isotherm (~ 22 Å²/molecule) compared to the 25 °C isotherm (~ 32 Å²/molecule).

DPPC and Gm1. The phase behavior of the phospho- and glycolipid monolayers at the air–water interface was also characterized by recording π - A isotherms for the Gm1 and DPPC monolayers on a mildly acidic subphase. Representative compression isotherms from those obtained in several measurements for the DPPC and Gm1 monolayer films at 15 and 25 °C are shown in Figure 2a and b, respectively. The 25 °C isotherms, for both DPPC and Gm1, were found to be in excellent agreement with those reported previously.⁴⁰ In the 25 °C isotherm for DPPC, all five regions (I–V) are easily distinguished. A flat portion (I) of the isotherm at 0 mN/m for molecular area > 100 Å²/molecule is followed by the first limb of increasing surface pressure (II) between 90 and 70 Å²/molecule. The limb region is then followed by a well-defined plateau region (III) between 70 and 55 Å²/molecule, which

(39) (a) Bierbaum, K.; Grunze, M.; Baski, A. A.; Chi, L. F.; Schrepp, W.; Fuchs, H. *Langmuir* **1995**, *11*, 2143–2150. (b) Schwartz, D. K.; Steinberg, S.; Israelachvili, J.; Zasadzinski, J. A. N. *Phys. Rev. Lett.* **1992**, *69*, 3354–3357.

(40) See, for example, for DPPC: (a) Morgan, H.; Taylor, D. M.; Oliveira, O. M. *Biochim. Biophys. Acta* **1991**, *1062*, 149–157. (b) Phillips, M. C.; Chapman, D. *Biochim. Biophys. Acta* **1968**, *163*, 301. (c) Gorwyn, D.; Barnes, G. T. *Langmuir* **1990**, *6*, 222–230. For Gm1: (d) Luckham, P.; Wood, J.; Froggatt, S.; Swart, R. *J. Colloid Interface Sci.* **1993**, *156*, 164–172. (e) Cheng, Q.; Stevens, R. C. *Chem. Phys. Lipids* **1997**, *87*, 41–53. (f) Maggio, B.; Cumar, F. A.; Caputto, R. *Biochem. J.* **1978**, *171*, 559–565.

Table 1. Collapse Pressure (mN/m) and A_0 Values ($\text{\AA}^2/\text{molecule}$) for the Three Monolayers OTS, DPPC, and Gm1 at the Air–Water Interface^a

molecule	collapse pressure		A_0	
	15 °C	25 °C	15 °C	25 °C
OTS	56		22	32
DPPC	57	51	53	63
Gm1	64	60	46	61

^a The subphase was mildly acidic at pH = 5.6.

is replaced by a second limb of rapidly rising surface pressure (IV) between 55 and 40 $\text{\AA}^2/\text{molecule}$, ultimately leading to film collapse (V) above ~ 51 mN/m. The 25 °C trace for the Gm1 monolayer similarly shows all corresponding regions between the molecular areas 85 and 40 $\text{\AA}^2/\text{molecule}$, except that the plateau region (III) is significantly narrower, replaced essentially by a sharp inflection point. In comparison, for both DPPC and Gm1, the isotherm data at lower (15 °C) temperature show marked differences. First, in the case of DPPC, the observation of a single steep rise in the slope of the curve at ~ 55 $\text{\AA}^2/\text{molecule}$ indicates that the monolayer phase upon compression undergoes a single main phase transition from the G to the LC phase before collapse. For Gm1, on the other hand, the temperature dependence is less pronounced and only sharpening of the inflection point characterizing the LE–LC phase transition is evident. Limiting surface areas or A_0 values for DPPC and Gm1 interfacial films are also summarized in Table 1. The 15 °C isotherm values of ~ 50 $\text{\AA}^2/\text{molecule}$ for the two lipids are slightly but distinctly lower than the values of ~ 60 $\text{\AA}^2/\text{molecule}$ obtained for the 25 °C isotherm, suggesting improved packing of the molecules upon lowering the subphase temperature. In comparison with the values of ~ 36 – 40 $\text{\AA}^2/\text{molecule}$ reported in the literature for the densest phases of two-chain amphiphiles,³⁸ the larger values obtained in the present cases reflect the packing constraints imposed by the nature of the head-groups in the two lipids. The structural consequences of the above are discussed below.

3.2. Single-Wavelength Ellipsometry. *OTS.* The ellipsometrically determined OTS film thicknesses for five different OTS/SiO₂/Si samples prepared by LB transfers were found to fall in the narrow range 25–27 Å when estimated using the isotropic chain model. Application of the more rigorous anisotropic model (see Experimental Section) yielded systematically lower values in the range 23–25 Å. In previous studies,⁴¹ determined solution-phase assembled OTS monolayer thicknesses have been variously reported between 23 and 28 Å. The presently obtained values are quite consistent with these previous reports but have slightly higher values of the average thickness. We estimate this shift to arise from a slightly better packing of the OTS monolayers and/or a better defined prewetting water layer at the film–substrate interface caused by the transfer of a prepolymerized OTS monolayer from the air–water interface.⁴² By comparison with the molecular thickness of 26.2 Å estimated for a fully extended all-trans chain conformation using a simple molecular mechanics model, our results are entirely consistent with the formation of a near-complete single

monolayer of OTS molecules with no appreciable tilt of the aliphatic chains.

DPPC and Gm1. The total DPPC film thickness l , based on an isotropic model (see Experimental Section), was estimated to be 29.0 (± 2) Å. An error of 0.05 units in the refractive index assignment was found to introduce the uncertainty ~ 1.5 Å in the film thickness estimations, well within the ± 2 Å experimental error. More rigorous anisotropic calculations performed using separate optical layers for the chain and the head-group regions (see Experimental Section) yielded the overall film thickness for the DPPC layer $l = 25.5$ (± 2) Å. In these calculations, the assignment of the PC head-group thickness l_h to values ranging from 5 to 9 Å led to the chain-layer thickness changing from 20.5 to 16.5 Å, thereby yielding for all cases the total DPPC film thickness ~ 25.5 Å. This value is in good general agreement with the values 24–26 Å obtained in previous ellipsometric and neutron reflectivity measurements for DPPC monolayers in condensed states at the air–water interface.³² It is clear that the thickness contribution from head-group and tail regions, the collective molecular tilt, and the structural anisotropy are inherently coupled and that the present calculations alone do not independently establish the individual contributions from each. Later in the manuscript, using infrared data analysis (see below), we independently determine the average chain structure for the DPPC layer to be fully extended in an all-trans conformation with the tilt of the average chain ~ 36 (± 3)°. Using these data, we obtain the chain-layer thickness 15.5 Å estimated as $l_m \cos(\theta)$, where l_m ($= 19.1$ Å) is the theoretical molecular length of the palmitoyl chain in the all-trans conformational state and θ is the tilt angle. Implementation of the above values in the present ellipsometric data analysis in conjunction with the anisotropic model yields the head-group thickness ~ 7.8 Å, quite consistent with the previous X-ray estimates^{32b} $l_h = 7.4$ Å and $l_t = 16.8$ Å for the most condensed phase of the DPPC monolayer at an air–water interface. However, the overall DPPC layer thickness 15.5 + 7.8 = 23.3 Å from this model is slightly smaller than the above estimates.

For the glycolipid monolayer Gm1, the isotropic three-layer calculations of ellipsometric data give the film thickness 45 (± 2) Å. The refractive index value 1.403 + 0i reported from the analysis of surface force apparatus measurements by Wood and co-workers³³ was used. This lower value of refractive index is quite consistent with the large pentasaccharide (PS) head-group in the Gm1 monolayer. Retention of water between the head-groups causes the overall refractive index to approach values close to that of bulk water ($n = 1.3313 + 0i$). An inaccuracy of 0.05 units in refractive index was noted to introduce an uncertainty of 2 Å in the estimated film thicknesses. The four-layer anisotropic model implementing anisotropic optical functions for the chain region ($n_o = 1.484$, $n_e = 1.559$) and the tail slab thicknesses $15 \leq l_t \leq 19$ Å yielded head-group thicknesses at $n = 1.3313 + 0i$ between 30 and 26 Å with the overall thickness ~ 45.3 (± 2) Å. These values are generally consistent with the estimates of 100 Å reported for single bilayers⁴³ or ~ 50 Å for the monolayer leaf of Gm1 molecules using X-ray diffraction, surface force measurements, and molecular models. Given the lack of independent information regarding the thicknesses of the head or tail regions, no further analysis of the present data was carried out.

(41) Wasserman, S. R.; Whitesides, G. M.; Tidswell, I. M.; Ocko, B. M.; Pershan, P. S.; Axe, J. D. *J. Am. Chem. Soc.* **1989**, *111*, 5852–5861.

(42) Interfacial monolayers of prepolymerized long-chain silane precursors are recently demonstrated to adhere to a molecularly thin surface water layer. The presence of this layer, estimated to be ~ 2 – 4 Å, is consistent with the higher values of 24–28 Å observed in ellipsometric measurements of the transferred monolayers.

(43) (a) Leneveu, D. M.; Rand, R. P.; Parsegian, V. A.; Gindell, D. *Biophys. J.* **1977**, *18*, 207. (b) Cowley, A. C.; Fuller, N. L.; Rand, R. P.; Parsegian, V. A. *Biochemistry* **1978**, *17*, 3163. (c) Wynn, C. H.; Robson, B. *J. Theor. Biol.* **1986**, *123*, 221.

3.3. Wetting Measurements. *OTS.* Surface wetting of OTS monolayers was determined using water and four apolar *n*-alkanes as probe liquids. Advancing and receding water contact angle values of $113 (\pm 3)^\circ$ and $106 (\pm 3)^\circ$ were measured. Contact angles due to apolar *n*-alkanes led to the critical surface tension values 21.3 dyn/cm. Both these values are in excellent agreement with the previously published values for solution-phase assembled OTS monolayers.⁴⁴ From comparison with the lowest values of 20–21 dyn/cm reported for a fully methylated surface,²⁶ combined with high water contact angles with small hysteresis, we infer that the present samples expose dominantly CH_3 groups in a dense homogeneous array covering the surface of oxidized silicon (SiO_2/Si) in a continuous manner.

DPPC and Gm1. The wetting of lipid layers was not characterized explicitly. However, visual observations regarding the wetting of the film surfaces were made during the horizontal transfer of the samples. Upon withdrawal from the contact with the air–water interface, the meniscus was noted to break abruptly, leaving little or no visible water layer at the coated substrates, suggesting autophobicity. Upon contacting the samples with the air–water interface without the lipid layer, spreading of water at the sample surfaces posing a contact angle of below 10° was noted to occur.

3.4. Infrared Spectroscopy. *Observed Spectra.* FTIR spectroscopy was used to determine the average structural attributes of the asymmetric bilayers, including chain-conformational order, chain-orientational order, surface coverage, and molecular packing, for each of the two leaves of the HBM systems examined here. These data are discussed in turn below.

OTS. Figure 3 displays a representative spectrum obtained for the transferred LB films of surface hydrolyzed, prepolymerized monolayers of OTS on the oxidized silicon substrate. The figure also includes in the top panel the infrared spectrum of bulk or 3-dimensionally hydrolyzed polymers obtained from OTS molecules⁴⁵ for comparison purposes. The peaks in the high-frequency regions of these spectra ($2700\text{--}3100\text{ cm}^{-1}$), which contain three well-resolved peaks at approximately 2850, 2918, and 2956 cm^{-1} , are straightforwardly assigned to the various stretching modes of the aliphatic chain⁴⁶ (Table 2). The details of these absorptions, including the exact locations of peaks, their full-widths at half-maximum, and the relative intensity distributions, are in good general agreement with the earlier reports of infrared spectra for the highest quality OTS monolayers prepared by solution-phase self-assembly methods.⁴⁷ Mode assignments and structural implications from this spectral region, in terms of collective chain-tilt, molecular conformation, and dense packing of C–C–C backbone planes, have also been previously made⁴⁷ (and will not be repeated here), and it was concluded that the chains are packed in a dominantly all-trans conformation with a near-untilted orientation of polymethylene chains. The asymmetric band with a maximum at $\sim 1468\text{ cm}^{-1}$ can be assigned to overlapping

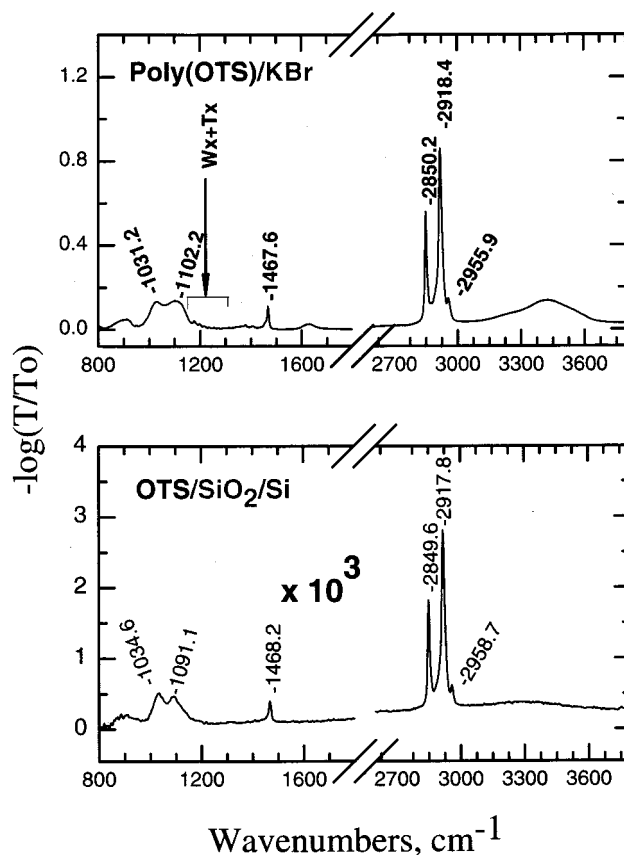


Figure 3. Mid-infrared difference spectra ($800\text{--}3650\text{ cm}^{-1}$) of LB-transferred OTS monolayers on an SiO_2/Si substrate (bottom panel) and bulk-hydrolyzed *n*-octadecylsiloxane pressed in a KBr matrix (top panel).

contributions from CH_2 scissoring deformation ($\sim 1467\text{ cm}^{-1}$) and CH_3 methyl antisymmetric bending modes ($\sim 1455\text{ cm}^{-1}$). To further delineate the contribution from each mode, the observed peak was fit to two peaks using standard fitting routines. The results of this analysis converged at a two-peak fit with a contributing broad peak (fwhm $\sim 33\text{ cm}^{-1}$) centered at 1456 cm^{-1} and a sharp peak (fwhm 9.9 cm^{-1}) centered at 1468.1 cm^{-1} . The observed sharpness of the CH_2 scissoring peak in conjunction with the singlet (no factor group splitting) nature of the peak is strongly suggestive of the presence of one chain type per unit cell packed in a hexagonal or triclinic arrangement⁴⁸ and provides a strong additional confirmation of the all-trans structure of densely packed alkyl chains. However, the progression bands due to the wag–twist motion of all-trans ordered chains are not clearly observed ($1100\text{--}1300\text{ cm}^{-1}$) in the monolayer spectra.⁴⁹ We have established using spectral calculations (not detailed here) that the most intense and fully resolved wag–twist mode at $\sim 1273\text{ cm}^{-1}$ would result in spectral intensities for the present experimental geometry below 2×10^{-5} units in $-\log(T/T_0)$ absorption units, comparable to the noise level in our spectra. Therefore, their absence from our spectra should be regarded as inconclusive. Taken together, the IR evidence of chain order suggests the formation of a near-complete OTS monolayer wherein the average alkyl chain exists in an all-trans conformation in a nearly-untilted

(44) Brzoska, J. B.; Shahidzadeh, N.; Rondelez, F. *Nature* **1992**, *360*, 719–721.

(45) Parikh, A. N.; Schivley, M. A.; Koo, E.; Seshadri, K.; Aurentz, D.; Mueller, K.; Allara, D. L. *J. Am. Chem. Soc.* **1997**, *119*, 3135–3143.

(46) (a) Snyder, R. G.; Schachtschneider, J. H. *Spectrochim. Acta* **1963**, *19*, 85–116. (b) MacPhail, R. A.; Strauss, H. L.; Snyder, R. G.; Elliger, C. A. *J. Phys. Chem.* **1982**, *88*, 334–341. (c) Snyder, R. G.; Hsu, S. L.; Krimm, S. *Spectrochim. Acta, Part A* **1978**, *34*, 395–406. (d) Hill, I. R.; Lewin, I. W. *J. Chem. Phys.* **1979**, *70*, 842–851.

(47) (a) Parikh, A. N.; Allara, D. L.; Ben Azouz, I.; Rondelez, F. *J. Phys. Chem.* **1994**, *98*, 7577–7590. (b) Allara, D. L.; Parikh, A. N.; Rondelez, F. *Langmuir* **1995**, *11*, 2357–2360. (c) Hoffmann, H.; Mayer, U.; Krischahntz, A. *Langmuir* **1995**, *11*, 1304–1312.

(48) (a) Chapman, D. *Trans. Faraday Soc.* **1965**, *61*, 2656. (b) Casal, H. L.; Mantsch, H. H.; Cameron, D. G.; Synder, R. G. *J. Chem. Phys.* **1982**, *77*, 2825.

(49) Bellamy, L. J. *The Infrared Spectra of Complex Molecules*; Chapman and Hall: London, 1975; pp 374–383.

Table 2. Identification and Assignment of Polymethylene Chain Modes to the Observed Infrared Peak Maxima in Wavenumbers (cm⁻¹) for the Surface Monolayer (m) and the Corresponding Polycrystalline Bulk (b) States of *n*-Octadecylsiloxane, DPPC, and Gm1 Molecules

vibrational mode ^a	obsd peak maximum, cm ⁻¹					
	OTS _b	OTS _m	DPPC _b	DPPC _m	Gm1 _b	Gm1 _m
asym CH ₃ str (ip); r _b ⁻	2955.9	2958.7	2956.7	2956.5	2957.5	2952.6
antisym CH ₂ str (op); d ⁻	2918.4	2917.8	2918.1	2916.8	2924.1	2916.8
antisym CH ₃ str (ip); r ⁺	2873.7	2872.9	2873.4	2872.8 (w)	2873.9 (w)	2872.2
sym CH ₂ str (ip); d ⁺	2850.2	2849.6	2850.1	2849.5	2853.7	2849.5
asym CH ₃ def; α	1457.5 (sh)	1458.2 (sh)	1457.0	1454.1 (sh)	1457.3 (sh)	
CH ₂ HCH bend (scissor); δ	1467.6	1468.2	1468.4	1467.5	1468.1	1467.3
sym CH ₃ def (umbrella); U	1378.2	1379.0	1378.0	1381 (vw)	1383.2	1378.3
CH ₂ wag + twist; T _x + W _x	1309, 1274, 1256, 1236, 1217, 1197, 1177	1275, 1261, 1217.7, — (vww)	1284 (sh), 1263.9 (sh), 1224, 1200, 1179	1282, 1260 (s), 1245, 1225, 1179, 1168, 1148, 1128 (all sh)	—, 1172, 1198	
CH ₂ end-gauche wag; W(t _m g)	1341.6 (vw)	broad envelope	1343.8 (vw)	1348.2 (vw)	1344.6	
CH ₂ kink wag; W(gt _m g ^t)	1304 (vw), 1365 (vw)	1300–1345	1367 (sh) 1309	1309 (br), 1369 (vw)	1308.2	
CH ₂ rock; P	720.8		721.9, 764.6, 824.8, 874.4		721.1	

^a str, stretching; br, broad; w, weak; vw, very weak; sh, shoulder; def, deformation; sym, symmetric.

orientation and experiences a crystalline-like environment in hexagonal packing.

Details of the head-group modes in the lower frequency region of the spectra have not been fully investigated in previous studies⁵⁰ and thus provide new opportunities to deduce the head-group structure of the siloxane backbones in the LB monolayers of OTS/SiO₂/Si from the present data. The region is characterized by a weak but reproducible envelope at ~890 cm⁻¹ and a strong distinct doublet with peak-maxima at 1034 and 1091 cm⁻¹. Comparable features are also observed for the 3-dimensionally hydrolyzed OTS molecules. (See Figure 3.) Mode assignments for these head-group vibrations are made in comparison with the previously made assignments for bulk organosiloxanes⁵¹ and water-related vibrational modes in amorphous silica.⁵² The presence of the weak 890 cm⁻¹ band reveals that a small fraction of unreacted silanols exists while the more intense doublet characterizes the dominant Si–O–Si cross-linking. Previous studies of a variety of bulk organosiloxanes suggest that the Si–O–Si peaks appear as a broad feature between 1000 and 1100 cm⁻¹ in simple disiloxanes and become a progressively better resolved doublet in long-chain linear polysiloxanes. Cyclic oligomeric siloxanes also absorb in the same region with a characteristic band near 1100 cm⁻¹ for large oligomers. The present observations of a well-resolved doublet with maxima at 1035 and 1091 cm⁻¹ are consistent with the formation of highly cross-linked one- or two-dimensional Si–O–Si networks. Further, Tripp and co-workers⁵³ have recently reported that when long-chain trifunctional silanes bind to silica beads, the stretching of Si_(s)–O–Si (where Si_(s) is a Si atom from the bead surface) occurs as a distinct peak at 1060 cm⁻¹. Our data do not show such a peak,⁵⁴ suggesting that condensation with the surface is low, as is expected, since prior to deposition equilibrium

two-dimensional condensation must occur at the air–water interface. As revealed by the changes in this spectral signature, the dependence of the Si–O–Si backbone structure on the properties of the aqueous subphase is pronounced and can be usefully employed to manipulate the monolayer architecture. A systematic investigation of these effects is beyond the scope of the present paper and will be separately reported.

DPPC and Gm1. Representative difference spectra for the DPPC and the Gm1 layers obtained by referencing the spectra of OTS/SiO₂/Si samples to those obtained for DPPC/OTS/SiO₂/Si and Gm1/OTS/SiO₂/Si are shown in Figures 4 and 5, respectively. Also shown in each figure are the corresponding spectra of the bulk polycrystalline DPPC and Gm1 solids dispersed in a KBr matrix.

Even a casual survey of the two figures reveals unambiguously that all dominant spectral features of the bulk samples are reproduced in the monolayer spectra of DPPC and Gm1, proving that the structural integrity and the basic inter- and intramolecular interactions that dictate the spectral behavior in the bulk state are not significantly altered during the monolayer transfers of lipids at oxide substrates in the HBM environment. Further, since no appreciable asymmetry or broadening or negative contributions appear, it is evident that the deposition of the lipid outer layer does not appreciably perturb the structural integrity of the initial silane layer. To further confirm this inference, control experiments utilizing perdeuterated DPPC lipid (spectra not shown here) were performed. The spectra obtained in these control measurements did not show any absorption (+ or –) in the C–H stretching region, providing conclusive evidence in support of the above assertion. The detailed assignment of the observed peaks with characteristic vibrational modes based on previous studies of DPPC⁵⁵ and Gm1 molecules is summarized in Tables 2 and 3. The specific assignment of selected peaks, grouped together as acyl chain modes and head-group modes for simplicity, as well as their structural implications, is discussed in turn below.

Acyl Chain Modes. The exact location of the methylene symmetric and antisymmetric stretching, d⁺ and d⁻, modes is a well-known diagnostic marker in the determination

(50) The backbone modes observed so clearly in the present spectra were not analyzed in previous studies, presumably due to complications from the changes in the Si substrate phonon structures. Here, however, we were able to systematically eliminate substrate contributions quantitatively and be able to resolve the Si–O modes by simply realigning the filmed substrates in the optical path of the spectrometer in the identical position for each reference and sample spectra collection.

(51) Smith, A. L.; Anderson, D. R. *Appl. Spectrosc.* **1984**, *38*, 822–825.

(52) Davis, K. M.; Tomozawa, M. *J. Non-Cryst. Solids* **1996**, *201*, 177–198 and selected references therein.

(53) Tripp, C. P.; Hair, M. L. *Langmuir* **1995**, *11*, 1215–1219.

(54) Curve fitting of the Si–O–Si peaks revealed presence of at least three peaks at 1028, 1089, and 1124 cm⁻¹ in our monolayer spectra.

(55) See, for example: (a) Fringelli, U. P.; Gunthard, Hs. H. In *Membrane Spectroscopy*; Grell, E., Ed.; Springer-Verlag: Berlin, 1981; pp 270–333. (b) Cameron, D. G.; Casal, H. L.; Mantsch, H. H. *Biochemistry* **1980**, *19*, 3665–3672. (c) Snyder, R. G.; Liang, G. L.; Strauss, H. L.; Mendelsohn, R. *Biophys. J.* **1996**, *71*, 3186–3198.

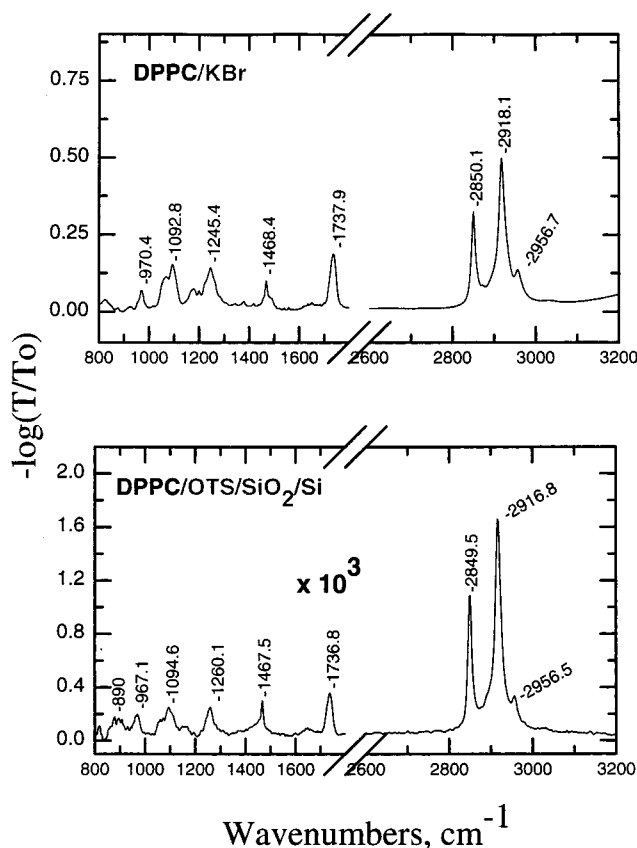


Figure 4. Mid-infrared difference spectra ($800\text{--}3650\text{ cm}^{-1}$) of a DPPC overlayer in the DPPC/OTS/SiO₂/Si HBM environment (bottom panel) and a bulk polycrystalline powder sample of DPPC pressed in a KBr matrix (top panel).

of chain-conformational order. In solid crystalline phases, the symmetric methylene stretches (d^+) of alkyl chains absorb between 2848 and 2850 cm^{-1} , and the antisymmetric stretches (d^-) occur between 2916 and 2918 cm^{-1} . For a conformationally disordered liquid phase, however, absorptions due to d^+ and d^- modes occur at the distinctly higher ranges $2856\text{--}2858\text{ cm}^{-1}$ and $2924\text{--}2928\text{ cm}^{-1}$, respectively. The observed frequencies 2849.5 and 2916.8 cm^{-1} for both Gm1 and DPPC are clearly consistent with those characterizing a solid crystalline phase, suggesting the presence of essentially all-trans ordered chains in a dense molecular environment comparable to that of crystalline n -alkanes. The low $7\text{--}10\text{ cm}^{-1}$ peak widths measured for these peaks are also consistent with this conclusion. Further, comparisons with the precise locations of d^+ and d^- modes in the KBr spectra of the bulk analogues show that while the acyl chains in DPPC monolayers in the HBMs experience a molecular environment comparable to the bulk crystalline state, these chains in Gm1 monolayers are noticeably different from their bulk counterparts. The solid phase of Gm1 in a KBr dispersion shows broad d^+ and d^- absorptions at the higher frequencies 2854 and 2924 cm^{-1} , respectively, suggesting a liquid-like organization of the acyl chains that sharply contrasts the crystalline-like environment deduced for Gm1 in the HBM.

The asymmetric band observed at $\sim 1467\text{ cm}^{-1}$ assigned to the methylene scissoring mode for both Gm1 and DPPC layers provides additional information regarding the packing of acyl chains. The appearance of the single band for the scissoring mode directly suggests the absence of factor-group splitting, and consequently the unit cell is comprised of a single type of acyl chains in triclinic or

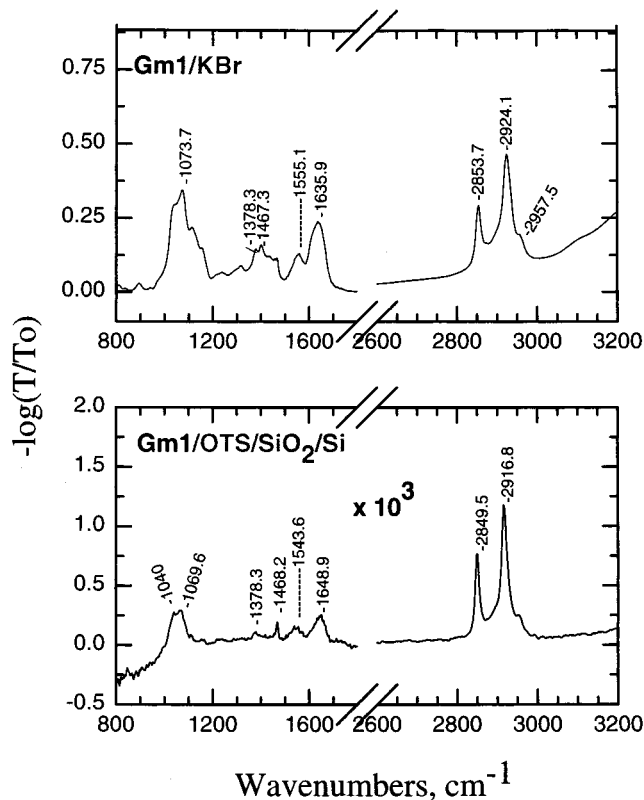


Figure 5. Mid-infrared difference spectra ($800\text{--}3650\text{ cm}^{-1}$) of a Gm1 overlayer in the Gm1/OTS/SiO₂/Si HBM environment (bottom panel) and a bulk powder sample of Gm1 pressed in a KBr matrix (top panel).

hexagonal packing.⁵⁶ Additionally, the observed full-width at half-maximum $13\text{--}14\text{ cm}^{-1}$ is intermediate to the values $8\text{--}10\text{ cm}^{-1}$ reported for the dense, crystalline packing of all-trans hydrocarbon chains and the values $18\text{--}25\text{ cm}^{-1}$ for disordered alkyl chains.⁵⁷ One likely possibility for the chain packing consistent with the evidence above would require the chains to be packed in a rotator or symmetrical hexagonal phase with an expanded lattice. These phases are known to be composed of a single type of chains in the unit cell, undergoing hindered rotational or twisting motions about their long axis.⁵⁸

A supportive requirement of the all-trans structure deduced above is the presence of progression of the wag-twist modes due to CH₂ groups in the $1100\text{--}1380\text{ cm}^{-1}$ region. The presence of the weak fine structure clearly seen in the bulk spectra of Gm1 and DPPC and only seen as weak vestiges in the monolayer spectra is tentatively assigned to the progression modes. In both cases, the peaks are virtually masked by pronounced absorptions from the head-group modes (see below). The low intensities of the wag-twist modes for these molecules can also be a result of the attenuation of the progression mode dipole strengths of the polymethylene sequences by polar end group(s). It is instructive to note here that the progression bands for the OTS monolayers could not be easily distinguished presumably due to lowered dipole strengths of methylene sequences due to the presence of attached siloxane head-groups.

Head-group Modes. The bulk of the bands observed in the lower frequency region of the spectra for DPPC and

(56) Snyder, R. G. *J. Mol. Spectrosc.* **1961**, *7*, 1161–1185.

(57) (a) Cameron, D. G.; Casal, H. L.; Mantsch, H. H.; Boulanger, Y.; Smith, I. C. P. *Biophys. J.* **1981**, *35*, 1–16. (b) Cameron, D. G.; Casal, H. L.; Mantsch, H. H.; Snyder, R. G. *J. Chem. Phys.* **1982**, *77*, 2825.

(58) Chapman, D. *Trans. Faraday Soc.* **1965**, *61*, 2656.

Table 3. Identification and Assignment of Head-Group Modes to the Observed Infrared Peak Maxima in Wavenumbers (cm^{-1}) for the Surface Monolayer (m) and the Corresponding Polycrystalline Bulk (b) States of *n*-Octadecylsiloxane, DPPC, and Gm1 Molecules

vibrational mode ^a	obsd peak maximum, cm^{-1}					
	OTS _b ^b	OTS _m ^b	DPPC _b	DPPC _m	Gm1 _b	Gm1 _m
	1102.3, 1031.8 (br env)	1091.1, 1034.6 (br env)				
	949.6	949.6 (vw)				
	902.2	900–921 (br)				
ester C=O str			1737.2	1736.8		
PO ₂ ⁻ asym str			1245.4	1260.1		
			(s, br)	(s, br)		
PO ₂ ⁻ sym str			1092.8	1094.7		
ester C–O sym str + C–C str			1068.9 (sh)	1073.2 (sh)		
C–C str			970.4	969.3		
HN–C=O amide mixed modes + COO ⁻ sym and asym str ^c					1617, 1635.2, 1645.6, 1652.5	1590–1680 (br, s), 1666, 1650, 1633, 1615
					1249.1	
CO str, in saturated C–OH bonds ^c					1172.9, 1198.4	
CO str, in saturated C–OH bonds ^c					1094.3 (s, Br), 1063, 968.5	1040.1, 1069.6 (s, br), 1109.6 (w)
					819.2, 873.6, 925.2	821, 847, 865, 906, 926, 939.8

^a str, stretching; br, broad; w, weak; vw, very weak; sh, shoulder; def, deformation; sym, symmetric. ^b m, monolayer state; b, bulk polycrystalline state. ^c Obtained from the second derivative of the absorption spectrum.

Gm1 leaflets are assigned to specific vibrational modes due to the phosphocholine and pentasaccharide head-groups, respectively. A summary of the most discernible peaks and their mode assignments is also given in Table 3.

For DPPC, the positions and relative intensities of the bands in this region reflect the conformational variations in the PC head-group about the O–C–C–N framework. All but one of the observed features between the spectrum of bulk, microcrystalline DPPC and that of DPPC in HBMs are directly comparable, suggesting that the head-group structure in the two cases is virtually indistinguishable. The only major difference is seen in the position of the asymmetric phosphate stretch: in the HBM environment, the observed peak maximum at 1260 cm^{-1} contrasts with the 1245 cm^{-1} peak maximum for the KBr dispersion of the microcrystalline solid DPPC. This shift of 15 cm^{-1} can be correlated with differences in the hydration level of the two samples. The phosphate group is the major receptor of water hydrogen bonds. H-bonding interactions in the hydrated films with water are known to significantly lower the force constants of the PO₂⁻ symmetric stretching modes.^{55a} By comparison with hydration dependent studies of DPPC multilayers,⁵⁵ we conclude that the DPPC in the HBM environment has a highly dehydrated head-group comparable to 1–10% relative humidity, whereas the level of hydration in the KBr dispersion of solid DPPC is equivalent to that of multibilayers maintained at ~60% relative humidity. Such low hydration of the head-group region in the HBM could call into question the assumption made in the ellipsometric analysis that the head-group region's refractive index is near that of water. However, since the hydration of the head-group region is likely to be greater outside the extremely desiccating environment of a purged FTIR and since the ellipsometric analysis is only mildly sensitive to small changes in the head-group region's refractive index, the prior analysis is unlikely to be significantly affected.

The lower frequency region of Gm1 spectra also shows a corresponding series of peaks due to the carbohydrate head-group. A comparison of the bulk and the monolayer

spectra due to Gm1 shows the presence of related features in both spectra, confirming the integrity of the pentasaccharide head-group in the HBM environment. The strongest band observed in this region is a broad envelope in the $1000\text{--}1200\text{ cm}^{-1}$ region observed for both the bulk crystallites and monolayer samples. The overlapping bands in this region are assigned to CO stretching modes in the saturated C–OH groups of the pentasaccharide head-group. The two broad bands observed in the $1500\text{--}1700$ region are group-assigned to amide and carboxylate modes. It has been previously predicted that these arise from a maximum of three amide groups and one carboxylate mode.⁵⁹

Determination of Molecular Orientations by Spectral Calculations. *OTS.* Determination of dipolar and chain orientation in oxide-supported SAMs of OTS molecules using the C–H stretching modes in the infrared has been previously reported,⁴⁷ and it was concluded in that study that molecular chains are tilted at an average of $\sim 11^\circ$ from the surface normal. Our calculated tilt of $10 (\pm 3)^\circ$ is entirely in agreement. This finding is in good agreement with a number of other studies where the near vertical orientation of OTS chains was predicted using near-edge X-ray absorption fine structure, vibrational spectroscopy, X-ray reflectivity, and X-ray photoelectron spectroscopy measurements.⁶⁰

DPPC and Gm1. A comparison of the experimental and best-fit spectra calculated for the C–H stretching modes for DPPC and Gm1 in the hybrid bilayer environment is shown in Figure 6. The best-fit spectrum for DPPC was obtained for an average chain tilt of 36° and the best-fit Gm1 spectrum was obtained for a 7° chain tilt. On the basis of the experimental uncertainties involved in the determination of optical functions for the lipid layer, we believe these values for the model to be uncertain by $\pm 5^\circ$. It is further instructive to compare the line shapes of the

(59) (a) Muller, E.; Giehl, A.; Schwarzmann, G.; Sandhoff, K.; Blume, A. *Biophys. J.* **1996**, *71*, 1400–1421. (b) Hubner, W.; Mantsch, H. H. *Biophys. J.* **1991**, *59*, 1261–1272.

(60) Ulman, A. *Chem. Rev.* **1996**, *96*, 1533–1554 and selected references therein.

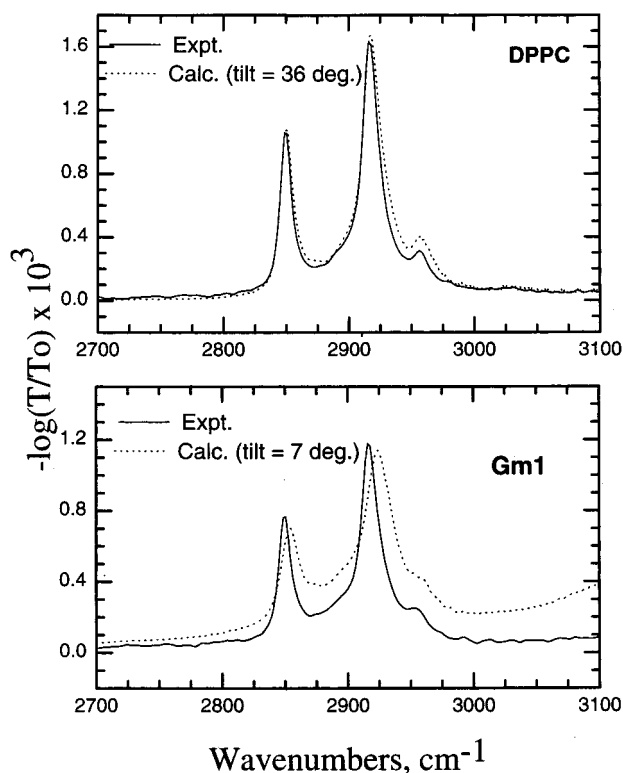


Figure 6. Comparison of the experimental difference spectra and the calculated best-fit spectra for (a) the DPPC monolayer in the DPPC/OTS/SiO₂/Si HBM and (b) the Gm1 monolayer in the Gm1/OTS/SiO₂/Si HBM. (See text for details.)

experimental and calculated spectra in the two cases. Excellent correspondence between the line widths in the case of DPPC reveal that the bulk microcrystalline DPPC provides a good reference state for the monolayer films in the HBM environment. In contrast, in the case of Gm1, the comparison between the experimental and calculated spectra is complicated by the differences in the chain-conformational properties between the bulk and the monolayer states. These differences lead to differences in the peak widths and a drop in the intensities of the intrinsic optical function spectra. This poor match in the line shapes (see Figure 6, lower panel) confirms the inadequacy of the Gm1 bulk state to correctly delineate the inter- and intramolecular interactions in the HBM environment. Further, the dependence of the spectral intensities on the chain-tilt angles below 20° in transmission experiments is known to be quite weak. Thus, we do not consider the present estimate of the 7° tilt angle in the case of Gm1 to be independently conclusive but note that this estimate is generally consistent with the untilted orientation of Gm1 chains concluded from the isotherm data above.

4. Discussion

4.1. General Remarks. The experimental evidence presented here confirms the formation of air-stable, lipid-alkylsiloxane bimolecular layers at the SiO₂/Si surface using successive vertical and horizontal transfers of precompressed Langmuir phases of alkylsiloxanes and lipids from the air-water interface. Vertical transfer of a single OTS layer provided a uniform hydrophobic template upon which the horizontal transfer of the precompressed lipid layer occurred. This conclusion is entirely consistent with previous studies of phospholipid-alkanethiol HBMs at Au surfaces by Plant and co-workers¹³ and thus serves to illustrate the extension of

the preparation protocol to oxide-based surfaces.⁶¹ Reproducibility in the transfer of the outer DPPC and Gm1 layers was found to depend strongly on a number of experimental parameters, most notably (1) template uniformity and hydrophobicity, (2) temperature of deposition, and (3) the surface pressure of the Langmuir phase. The uniform hydrophobicity of the silanized silicon substrates was found to be critically important in obtaining consistent reproducibility in the properties of the transferred lipid overlayers. Control experiments using hydrophobic templates of lower density monolayers of OTS⁶² resulted in larger sample-to-sample variabilities in the properties of the outer lipid leaflets. Similarly, large sample-to-sample variations were observed for the lipid layer properties when solution-phase self-assembly of OTS molecules was employed. We rationalize these observations to imply that the Langmuir-assisted transfers of OTS monolayers from a LC phase provide better hydrophobic templates for the horizontal lipid transfers. At present, it is unclear why we obtain less reproducibility in lipid transfers with the self-assembled silane monolayer templates, since all structural properties (infrared spectra, wetting, and ellipsometry) for the LB films of OTS deduced in the present study reflected little or no difference from previously reported properties of self-assembled OTS monolayers. A systematic study of the morphological and structural discrepancies between the self-assembled and Langmuir-Blodgett films of OTS monolayers is being currently pursued in our laboratory; however, our preliminary AFM measurements show large scale morphological differences between the samples prepared by these two techniques.⁶³

Next, we noted that, for the lipid layers, low deposition temperatures and high surface pressures for the Langmuir precursors favored the horizontal transfer. Attempts to transfer at low surface pressures, from a liquid-expanded (LE) phase, by the horizontal touch method were irreproducible and produced final films with erratic structural attributes for the lipid leaflets. It is also instructive to note that the spectroscopic evidence in the present study argues against any large scale restructuring of the inner OTS leaflet upon deposition of an outer leaflet. Meuse and co-workers¹³ have similarly noted only minor reconstruction of the alkanethiol layers upon deposition of the phospholipid layer. Finally, we note that the densely packed lipid outer layers were stable in air for several weeks but dissipated upon immersion into or retraction from aqueous media (i.e., upon passage through an air-water interface).

4.2. Structural Summary. All the spectroscopic and ellipsometry evidence presented can be reconciled in a general scenario of bimolecular structures for the HBMs of DPPC/OTS/SiO₂/Si and Gm1/OTS/SiO₂/Si wherein the outer Gm1 and DPPC leaflets remain as a structurally decoupled, noninterdigitated layer from the inner OTS layer with widely disparate structural properties. A schematic depiction of these general features is shown in Figure 7.

The structural uniformity and consistency of the inner OTS layer of the bimolecular HBM architecture implied in Figure 7 are amply substantiated in our data. An ellipsometrically derived average film thickness of ~25 Å

(61) A freshly oxidized glass surface and other wettable oxides provide bimolecular architectures comparable to those reported here.

(62) Low-density, islanded monolayers of OTS were prepared by Langmuir-Blodgett transfers at lower surface pressures of approximately 0, 5, 10, and 20 mN/m.

(63) Wang, R.; Beers, J. D.; Parikh, A. N.; Eberhardt, A. S.; Swanson, B. I. Unpublished material.

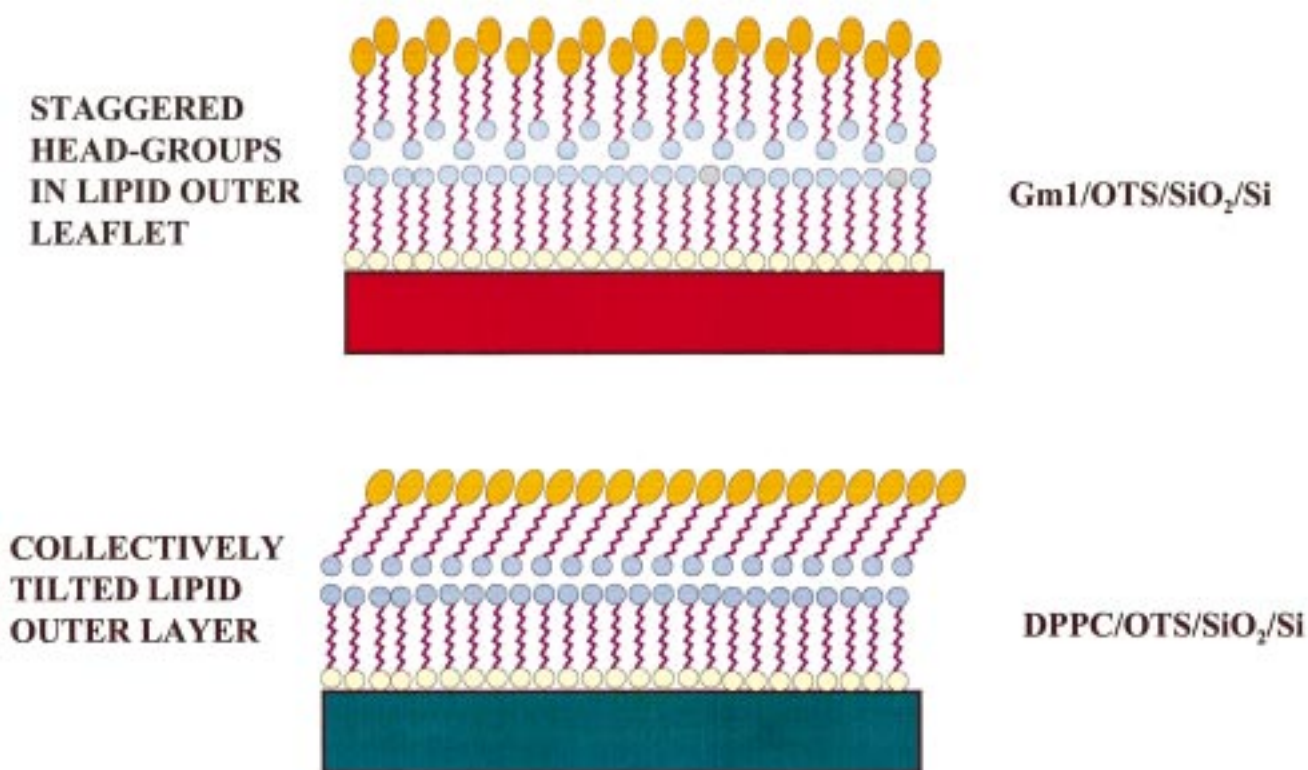


Figure 7. Cartoon depiction of the proposed bimolecular architecture for (a) the DPPC/OTS/SiO₂/Si HBM and (b) the Gm1/OTS/SiO₂/Si HBM, showing an exaggerated schematic view of the orientational, conformational, and topological characteristics.

in comparison with the molecular model estimate of 26.2 Å suggests the formation of a near-complete OTS monolayer comprised of fully extended all-trans octadecylsiloxane chain. Such a structure would require the uniform presence of end methyl groups at the outer interface. The critical surface tension value ~ 21 dyn/cm derived from contact angle data in the narrow range of values 20–22 dyn/cm reported for uniformly methylated surfaces is consistent in this regard. Both the vertical orientation (suggested on the basis of previously reported spectral calculations) and the essential dominance of the all-trans conformers in the polymethylene matrix (deduced primarily from the positions of d^+ and d^- methylene stretching modes) are well substantiated in the FTIR data analysis. Further, the product of the mean molecular area (~ 20 Å²/molecule) and the transfer ratio (~ 1) gives an estimate of ~ 20 Å²/molecule, in good agreement with the geometric requirement of 17–22 Å²/molecule for the densest packing of vertically oriented, all-trans chains. The head-group structure of the siloxanes reveals the presence of a polymerized component deduced from the appearance of strong Si–O–Si peaks in the FTIR data and the presence of weak, but distinct, unreacted Si–OH groups. In comparison with the estimate of ~ 150 for the extent of polymerization obtained from the π - A isotherm data,^{20b} it appears that the siloxy head-groups present a two-dimensionally cross-linked network.

The outer DPPC leaflet was found to be similarly conformationally ordered in the all-trans state at near-complete packing but with the average molecular chain in a tilted orientation canted at $\sim 36^\circ$ from the surface normal. In remarkable similarity with previously reported cant angle values of 34–36° for DPPC molecules in their native layered crystalline structures⁵⁹ and as monolayers at the air–water interface,⁶⁴ the present finding clearly shows that *the molecular environment of the HBMs does*

not influence the intrinsic packing at the highest coverages. It is obvious here that the tilt of the molecular chain is not induced by any symmetry requirements at the OTS template but is presumably a consequence of the steric and electrostatic constraints imposed by the phosphocholine head-group. By a comparison of the mean molecular area ~ 52 Å²/molecule estimated from the π - A isotherm data and the transfer ratio data with the densest packing of two-chain amphiphiles at ~ 38 –44 Å²/molecule, it is clear that the acyl chains in the condensed phase of the DPPC monolayer are less efficiently packed. The spectroscopically estimated tilt $\sim 36^\circ$ is geometrically consistent in that a collectively tilted organization of the chains at lower packing densities can afford an increased van der Waals contact.

The Gm1 layer was also found to be in a conformationally ordered state with the dominant population of all-trans conformers. The bulk Gm1 crystal at the same temperature however is conformationally disordered, as evident in the higher peak positions of d^+ and d^- methylene stretches. The improved conformational ordering in the Gm1 HBMs must be due to the extraneously applied lateral pressure at the air–water interface for the precursor film, which was evidently (transfer ratios near unity) conserved during the transfer to the substrates. The orientation of the alkyl chain determined using the electromagnetic model indicates that the polymethylene chains are vertically aligned with respect to the substrate surface at an $\sim 7^\circ$ cant angle. Further, the mean molecular area in the HBM environment, calculated using the area/molecule at the transfer condition and the transfer ratio data, suggests the value 46 Å²/molecule. This is comparable, on the higher end, to those obtained (38–44 Å²/molecule) for the dense, vertical packing of acyl chains.

(64) Stephens, S. M.; Dluhy, R. A. *Mikrochim. Acta* **1997**, S14, 455–457.

Interestingly, previous light-scattering studies of Gm1 micelles have indicated that the optimal carbohydrate head-group area for Gm1 is $\sim 98 \text{ \AA}^2$.⁶⁵ The observed area/molecule of 46 \AA^2 /molecule in the HBMs is strikingly lower and strongly suggests that the Gm1 head-groups in the HBMs are forced to extend away. The extended conformation of the pentasaccharide head-groups would most likely require them to adopt a staggered conformation³³ to relieve the excess head-group repulsion stress. Such a noncoplanar interfacial topology is rendered plausible because the head-group hydration provides a packing flexibility for the head-groups and staggering can improve the van der Waals contact between the chains. An interesting ramification of such a head-group packing is that the hydrophobic interface between the inner OTS and the outer Gm1 leaflets would also be corrugated, as schematically shown in Figure 7.

4.3. Formation Mechanism. The horizontal transfer of the lipid Langmuir phase at the hydrophobic templates can be understood in terms of the balance of two major interactions: (1) the long-range hydrophobic attraction between the methyl surface of the presilanized silicon substrate and the hydrophobic tails of the interfacial lipid precursor layer; and (2) the short-range repulsive interactions due to steric, electrostatic, and hydration forces. The successful transfer of the lipid layer from the air-water interface onto hydrophobic templates evident in the present study can be interpreted in terms of the dominance of the hydrophobic interaction between the two leaflets over the possible loss of hydration forces during the transfer.⁶⁶ In fact, several studies in the past have demonstrated that the long-range interactions between hydrophobic surfaces are often several orders of magnitude larger than the simple van der Waals attraction alone.⁶⁷ In view of these studies, it appears likely that the formation

(65) Cantu, L.; Corti, M.; Sonnino, S.; Tettamanti, G. *Chem. Phys. Lipids* **1986**, *41*, 315.

(66) The final films appear nominally dry, but the polar head-group region is not entirely dehydrated, rendering it difficult to assess if the transfer protocol incurred any significant loss of hydration-induced head-group stabilization. A systematic investigation of the hydration dependent, structural reconstructions in the HBMs at solid surfaces would be needed to further establish this point.

(67) See, for example: Rusling, J. F.; Kumosinski, T. F. *J. Phys. Chem.* **1995**, *99*, 9241-9247.

of HBM could be guided dominantly by the interlayer dispersive hydrophobic effect.

The almost complete structural independence observed between the outer lipid leaflets and the inner OTS layers provides additional insight into the interactions that control the layer structures in the bimolecular HBM architecture. For DPPC, the deduced structural characteristics suggest a close similarity to its native crystalline state, and for Gm1, the deduced structure appears analogous to those obtainable under high lateral pressures at the air-water interface. On the basis of the above, it appears that the inner OTS layer does not influence the intralayer packing in the outer lipid layers, which is almost solely determined by the head-group and chain-chain interactions between the lipid molecules.

5. Conclusions

The experimental evidence presented in this paper reveals that, by successive depositions of precompressed Langmuir monolayers of long-chain silanes and lipids, lipid-alkylsiloxane hybrid bimolecular architectures at oxidic substrates can be reproducibly prepared. In two specific cases, namely DPPC/OTS/SiO₂/Si and Gm1/OTS/SiO₂/Si, structural characterization using a combination of infrared spectroscopy, ellipsometry, and wetting measurements reveals the structural asymmetry between the two organic layers. The discommensurate nature of the two leaflets confirms the possibility of independently manipulating the molecular structure in each leaflet of supported hybrid bilayers, and the specific structural conformational, orientational, and topological features provide information regarding the relative importance of the interlayer hydrophobic interactions and the intralayer head-group and chain-chain interactions in controlling the hybrid, bimolecular film structure.

Acknowledgment. The authors gratefully acknowledge valuable discussions with C. Meuse and A. Plant (NIST). Contact angle data were obtained using an instrumental facility within the Materials Science & Technology Division of Los Alamos National Laboratory. Financial support for the research was provided by Los Alamos National Laboratory under the LDRD program for Optical Biosensors.

LA9813679